Sun Sensing for Planetary Rover Navigation

John Enright
Department of Aerospace Engineering
Ryerson University
Toronto, ON M5B2K3
416-979-5000x4174
jenright@ryerson.ca

Paul Furgale, Tim Barfoot
Institute for Aerospace Studies
University of Toronto
Toronto, ON M3H5T6
416-667-7700
{paul.furgale,tim.barfoot}@utoronto.ca

Abstract—In this paper, we present an experimental study of sun sensing as a rover navigational aid. Algorithms are outlined to determine (i) rover heading in an absolute reference frame and (ii) absolute rover position (i.e., latitude/longitude). Our sensor suite consists of a sun sensor, inclinometer, and clock (as well as ephemeris data). We describe a technique to determine ground-truth orientation in the field (without using a compass) and present a large number of experimental results (both in Toronto and on Devon Island) showing our ability to determine absolute rover heading to within a few degrees. We also present our preliminary results on determining absolute rover position.

TABLE OF CONTENTS

1. INTRODUCTION

Navigation for planetary rovers relies on integrated local measurements, most often from combinations of visual odometry, wheel tachometer readings, and inertial navigation sensors. These relative navigation schemes are subject to unbounded growth of errors over time/distance. Imagery from orbiting satellites can be used to provide global position corrections, but these updates are generally infrequent and introduce substantial latency if the imagery must be processed on the ground. Moreover, they give little information about the rover's heading. Absolute heading information can be calculated from digital compass readings, but the most likely targets for rover exploration (i.e. the moon and Mars) do not have useful magnetic fields. Measuring the sun direction with a high-accuracy sun sensor is an effective means of obtaining absolute orientation, and thereby reducing the drift in navigation accuracy during autonomous navigation.

978-1-4244-2622-5/09/$25.00 ©2009 IEEE
IEEEAC Paper #1340, Version 2.0, Updated 9 January 2009.

This paper examines the problem of rover navigation with the aid of sun sensors. We outline the mathematical basis of our heading (and position) determination and evaluate the algorithms on data collected through a number of field trials conducted in the summer of 2008. Tests were conducted at the University of Toronto Institute for Aerospace Studies (UTIAS) and on Devon Island in the Canadian Arctic as part the Haughton-Mars Project. The Devon Island terrain is a popular analog to the Martian surface and represents a good environment to evaluate rover navigation performance. Tests were conducted using a Sinclair Interplanetary SS-411 digital sun sensor and a suite of conventional rover sensors mounted on a mobile platform.

The paper is organized as follows. First, we review prior work on sun sensors for planetary rovers. Next, we present the theoretical development of our algorithms to determine both absolute rover heading and absolute global position. We then provide the details of our field testing campaign and experimental results. A conclusion follows.

2. PRIOR WORK

The inclusion of a sun sensor on future rover missions was one of the recommendations coming out of the 1997 Mars Pathfinder mission [1]. This recommendation was implemented on the 2004 Mars Exploration Rovers (MERs). Eisenman et al. [2] describe the method the MERs use to transform PanCam images into sun vectors. They do not describe the method of solving for orientation given the sun vectors. Ali et al. [3] also describe the uses of sun sensing on the MERs. The MERs use sun sensing in two different ways: (i) to update the heading of the rover and (ii) to update the full attitude of the rover (which is used to point the high gain antenna). The algorithms are not described, although they say that they use "QUEST" and cite Schuster and Oh [4]. Accuracy of the technique is not reported. We treat a similar problem in our Experiment 2 (Heading from Sun and Position) below. Maimone et al. [5] report that "As of January 2007, sun-locating commands have run more than 100 times on each rover"

Kuroda et al. [6] describe a lunar global/local localization method using sun vectors and Earth vectors. They perform simulations and find that, using sun and Earth vectors alone, they are able to estimate their global position on the moon to

within 0.5 km. The authors develop a method of linking consecutive global localization readings using dead-reckoning. They claim that this method increases the accuracy of the estimation to within 150 m. The authors do not report any results of hardware experiments nor do they include a model of inclinometer error in their simulations. It should be noted (for the purpose of comparison with our global position results) that the radius of the planetary body effects the accuracy of localization (i.e., a smaller radius results in a more accurate estimate).

Several JPL studies have also used rover-based sun sensing. Volpe [7] describes the field testing of the relative localization system on the Rocky 7 field rover. The sun sensor heading determination scheme limits the cross-track error to linear growth as the rover travels. Trebi-Ollennu et al. [8] describe the design and testing of a sun sensor on one of the FIDO rover platforms at JPL. They report errors in rover heading of a few degrees, which is comparable to our Experiments 1 and 2 below. Sigel and Wettergreen [9] perform some mathematical modeling and simulation for localization on the moon using a star tracker. They comment that the major source of error is the inclinometer. They also comment that the effect of the local gravity model on moon localization using this method should be negligible.

Deans et al. [10] develop a sun sensor based on a fisheye-lens firewire camera and an inclinometer bundled together. They describe their frames of reference, the calibration procedure for the system, and plot inclinometer and image residuals after calibration. To find orientation, they use a weighted least-squares cost function, which they optimize using a Levenberg-Marquardt algorithm. They assume their position on the planetary body is known. These assumptions are similar to the ones we make in our Experiment 1 (Heading from Sun, Gravity, and Position). Deans et al. state, "The sensor orientation is estimated to within a fraction of a degree, but we lack a simple and independent method for measuring the ground truth orientation with similar precision." The issue of ground-truth heading (particularly in a remote field setting) is a challenge that we attempt to address in the current paper. Deans et al. also state, "Results for position estimation for long traverses is beyond the scope of this paper, since position error depends on the fusion of multiple sources of information. These results will be reported elsewhere." The current paper provides some preliminary results on estimating global position using a sun sensor (Experiment 3).

Pingyuan et al. [11] describe a method of attitude determination on the moon using sun, Earth and gravity vectors. They formulate the problem similarly to the current paper and also use the q-method to solve for attitude. They test their system on one simulated traverse and conclude that their method will estimate orientation. This is similar to our Experiment 1 (Heading from Sun, Gravity, and Position), except that in Pingyuan et al., it is assumed the starting global position (i.e., latitude/longitude) is known and propagated through an odometry relative position estimate as the rover moves. This allows the global position to be known each time heading is estimated during the traverse.

Cozman and Krotkov [12] also use the "circles of equal altitude" method to solve for the position of a sun sensor. The authors develop a sun sensor using a camera and inclinometer. Altitude values are corrected for parallax and refraction. They minimize a least-squares cost function using a grid of initial guesses, keeping the best (lowest error) solution. They perform two experiments that are based on only two sun observations each. They report inclinometer as a major source of error. Their results are comparable to our Experiment 3 (Position and Heading from Sun and Gravity).

3. MATHEMATICAL FRAMEWORK

This section provides the mathematical framework for the analysis used in this paper. We first define the key frames of reference used in our measurements, explain the calculation of the predicted vectors, and then solve for the rover orientation that best matches the observations. We also consider how sensor data can be combined in different ways to solve for the relevent set of unknowns. Each configuration effectively defines a separate *experiment* (which are described below).

Frames of Reference

Working with vector observations is an exercise in frame transformations. In order to see how our sensor observations are related to predictions, we must understand the reference frames in which they are made. Six reference frames are of particular importance to this study (Table 1). The Earth-Centred Inertial (ECI) and Earth Centred Fixed (ECF) frame follow standard definitions. Rover heading and motion is best understood relative to the local topocentric frame. This frame is defined with respect to the local horizontal. Strictly speaking, gravity is measured normal to the geoid, but since the *deflection of the vertical* is always less than $0.01°$[13], we assume that gravity is also normal to the reference Earth ellipsoid. The remaining three frames are defined with respect to the sun sensor, inclinometer, and camera housings, respectively. For this study, we consider F to be the primary external frame and S to be the primary rover frame.

Because common notations differ slightly, it is worth mentioning our convention. Vectors and matrices are expressed in boldface (i.e., $\mathbf{x}_b$). Subscripts denote the frame of reference for the vector. All of our vector transformations are rotations, captured in transformation matrices of the form $\mathbf{C}_{ab}$, read as: the rotation from b to a. Hence, the transformation of a vector is written:

$$\mathbf{x}_a = \mathbf{C}_{ab}\mathbf{x}_b \tag{1}$$

It is often convenient to express frame transformations as a series of principal axis rotations. Using the shorthand $c_\theta \equiv \cos\theta$, and $s_\theta \equiv \sin\theta$, our notational convention defines the

Table 1. Relevant Frames of Reference

Frame	Notation	x-axis	y-axis	z-axis
Earth Centred Inertial (ECI)	I	Vernal Equinox		North Pole
Earth Centred Fixed (ECF)	F	Prime Meridian		North Pole
Topocentric	T	Local East	(Local North)	Opposite Gravity
Sun Sensor	S		Alignment Pins	Outward Normal
Inclinometer	G	Away From Connector		Outward Normal
Camera	C	Horizontal Pixels	Vertical Pixels	(Optical Axis)

three standard rotations:

$$\mathbf{R}_x(\theta) = \begin{bmatrix} 1 & 0 & 0 \\ 0 & c_\theta & -s_\theta \\ 0 & s_\theta & c_\theta \end{bmatrix}$$
$$\mathbf{R}_y(\theta) = \begin{bmatrix} c_\theta & 0 & s_\theta \\ 0 & 1 & 0 \\ -s_\theta & 0 & c_\theta \end{bmatrix} \quad (2)$$
$$\mathbf{R}_z(\theta) = \begin{bmatrix} c_\theta & -s_\theta & 0 \\ s_\theta & c_\theta & 0 \\ 0 & 0 & 1 \end{bmatrix}$$

The geometric interpretation of this convention is that if $\mathbf{C}_{ab} = \mathbf{R}_x(\theta)$, then b is obtained from a by a right-handed rotation of θ about the x-axis. Given these definitions, we next derive expressions for converting between the frames of interest.

The transformation from ECF to ECI is a simple rotation:

$$\mathbf{C}_{IF} = \mathbf{R}_z(\Psi) \quad (3)$$

where Ψ is the Greenwich Apparent Sidereal Time (GAST). In this study we use a 'low' accuracy algorithm [14] to calculate Ψ, which is accurate to about 1.3×10^{-4} degrees.

The transformation between T and F is a function of the rover longitude, λ, and latitude, ϕ. From the definitions of these frames we can show that

$$\mathbf{C}_{FT} = \mathbf{R}_z(\lambda)\,\mathbf{R}_y\left(\frac{\pi}{2} - \phi\right)\mathbf{R}_z\left(\frac{\pi}{2}\right). \quad (4)$$

Three further rotations in heading, α, pitch, β, and roll, γ, are used to calculate the transformation between the sun sensor and topocentric frames (the heading is measured counter clockwise from East):

$$\mathbf{C}_{TS} = \mathbf{R}_z(\alpha)\,\mathbf{R}_y(\beta)\,\mathbf{R}_x(\gamma) \quad (5)$$

The final frame transformations of note are between the sun sensor and the inclinometer and camera frames: $\mathbf{C}_{SG}$, $\mathbf{C}_{SC}$. This transformation captures the intended mounting geometry between the three sensors, as well as any misalignment between sensor axes. We do not assume a particular functional form for these matrices; they are obtained from calibration.

Sun and Gravity Vectors

Heading and position determination rests on our ability to relate measured vectors to predictions of what those vectors should be. The sun vector from the sun sensor can be related to the sun vector predicted from solar ephemeris. Likewise, gravity (as measured by our inclinometers) can be related to the expected gravity vector defined by our position.

The expected sun vector in ECI, $\mathbf{s}_I$, can be calculated from quasi-analytical models of solar ephemeris. Our sun sensor measurements are accurate to about 0.1°, so we can use a low accuracy prediction of the sun position. For this study we employ Meeus' solution [14], accurate to about 0.01° within a few centuries of the year 2000. These calculations rely on an accurate time reference, provided either by a local clock or obtained from GPS timestamps. Sun vectors are rotated into ECF using $\mathbf{C}_{FI}$, obtained from (3). Figure 1 compares the solar ephemeris predictions with the sun sensor data from a nine-hour test on September 10, 2008. The plots illustrate the observed range of solar motion, and the errors in the predictions over the course of the test. Irregularities in the observations near 15:45 and 17:15 are caused by partial cloud cover and gaps near 19:00 are caused by heavier cloud cover. Slow changes in the error suggest that some systematic biases are still present.

We transform $\mathbf{s}_I$ into ECF to give us the 'predicted sun vector', $\mathbf{s}_F$:

$$\mathbf{s}_F = \mathbf{C}_{FI}\mathbf{s}_I \quad (6)$$

The sun sensor itself provides $\mathbf{s}_S$, the 'measured sun vector'.

If rover position is known, the 'predicted gravity vector', $\mathbf{g}_F$, follows from simple geometry:

$$\mathbf{g}_F = \begin{bmatrix} c_\phi c_\lambda \\ c_\phi s_\lambda \\ s_\phi \end{bmatrix} \quad (7)$$

It is interesting to note that this expression holds regardless of whether ϕ is the geocentric or geodetic latitude.

The 'measured gravity vector', $\mathbf{g}_S$, can be calculated from the inclinometer readings. This instrument provides local pitch, β_G, and roll, γ_G, measurements such that

$$\mathbf{g}_G = \begin{bmatrix} s_{\beta_G} \\ -c_{\beta_G} s_{\gamma_G} \\ -c_{\beta_G} c_{\gamma_G} \end{bmatrix}. \quad (8)$$

We may transform the gravity vector into the sun sensor frame:

$$\mathbf{g}_S = \mathbf{C}_{SG}\mathbf{g}_G \quad (9)$$

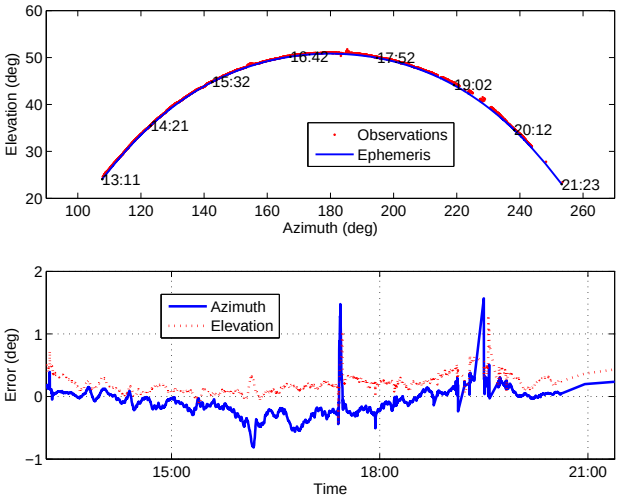

Figure 1. Predicted and observed sun track for a long-duration test. Azimuth angle is the compass bearing.

where $\mathbf{C}_{SG}$ is a calibration rotation matrix from the inclinometer frame to the sun sensor frame; we will describe how to determine this below.

Rotation Estimation

Our experiments differ in their use of the available instruments, but they share a common mathematical foundation. In each case, we must find the best estimate of $\mathbf{C}_{SF}$ that explains a set of observation vectors, $\mathbf{u}_{S_i}$, and predictions, $\mathbf{u}_{F_i}$. This can be written as a classic Wahba problem [15]. We wish to find the rotation matrix, $\mathbf{C}_{SF}$, that minimizes the scalar-weighted cost function

$$J\left(\mathbf{C}_{SF}\right) = \frac{1}{2}\sum_{i=1}^{m} a_i \left\|\mathbf{u}_{S_i} - \mathbf{C}_{SF}\mathbf{u}_{F_i}\right\|^2 \qquad (10)$$

where a_i is a scalar weight, m is the number of measurements, and $\|\cdot\|$ is the Euclidean norm. We solve this problem using Davenport's q-method [16]. Briefly summarizing this approach, we first concatenate the two sets of vectors into two matrices:

$$\mathbf{W} = \left[\begin{array}{cccc} \sqrt{a_1}\mathbf{u}_{S_1} & \sqrt{a_2}\mathbf{u}_{S_2} & \cdots & \sqrt{a_m}\mathbf{u}_{S_m} \end{array}\right] \qquad (11)$$

$$\mathbf{V} = \left[\begin{array}{cccc} \sqrt{a_1}\mathbf{u}_{F_1} & \sqrt{a_2}\mathbf{u}_{F_2} & \cdots & \sqrt{a_m}\mathbf{u}_{F_m} \end{array}\right] \qquad (12)$$

Then we calculate:

$$\mathbf{B} = \mathbf{W}\mathbf{V}^T \qquad (13)$$

$$\mathbf{Q} = \mathbf{B} + \mathbf{B}^T \qquad (14)$$

We extract the cyclic components of $\mathbf{B}$:

$$\mathbf{Z} = \left[\begin{array}{ccc} B_{23} - B_{32} & B_{31} - B_{13} & B_{12} - B_{21} \end{array}\right] \qquad (15)$$

where B_{ij} is the element of B in row i and column j. We also extract the trace of $\mathbf{B}$:

$$\sigma = \text{trace}\left(\mathbf{B}\right) \qquad (16)$$

Finally, we form the 4×4 matrix, $\mathbf{K}$:

$$\mathbf{K} = \left[\begin{array}{cc} \mathbf{Q} - \mathbf{1}\sigma & \mathbf{Z}^T \\ \mathbf{Z} & \sigma \end{array}\right] \qquad (17)$$

where $\mathbf{1}$ is a 3×3 identity matrix. The eigenvector corresponding to the largest eigenvalue of $\mathbf{K}$ is $\mathbf{q}_{SF}$, the 4×1 unit quaternion representing the best fit rotation from F to S. This quaternion is composed of a vector component, $\mathbf{q}_v$, and a scalar, q_s:

$$\mathbf{q}_{SF} = \left[\begin{array}{c} \mathbf{q}_v \\ q_s \end{array}\right] \qquad (18)$$

The desired rotation matrix, $\mathbf{C}_{SF}$, can be found from the quaternion:

$$\mathbf{C}_{SF} = \left(q_s^2 - \mathbf{q}_v^T\mathbf{q}_v\right)\mathbf{1} + 2\mathbf{q}_v\mathbf{q}_v^T - 2q_s\mathbf{q}_v^\times \qquad (19)$$

where the $\mathbf{q}_v^\times$ term is the skew-symmetric matrix formed from the components of $\mathbf{q}_v$:

$$\mathbf{q}_v^\times = \left[\begin{array}{ccc} 0 & -q_{v_3} & q_{v_2} \\ q_{v_3} & 0 & -q_{v_1} \\ -q_{v_2} & q_{v_1} & 0 \end{array}\right] \qquad (20)$$

At least two observations are required, but this method can be used with as many measurements as are available. In the context of this study, multiple sun vectors are helpful since the moving sun generates distinct, separate vectors. Multiple inclinometer readings do not add much new information since the gravity vector does not change. Instead, where multiple inclinometer readings are available, they are averaged to reduce noise before forming $\mathbf{W}$ and $\mathbf{V}$.

The q-method is simple and robust, especially when the processing is performed offline. For online implementations QUEST [4] or FOAM [17] may provide some computational advantages, but they were not considered in this study.

Experiment Description

One objective of this study is to compare the effectiveness of different sensor configurations on the measurement of heading and possibly global position as well. We carried out three distinct experiments:

1. Heading from Sun, Gravity, and Position
2. Heading from Sun and Position
3. Heading and Position, from Sun and Gravity.

Each experiment has different operational implications, in addition to a slightly different mathematical formulation. We examine each concept in turn.

Experiment 1: Heading from Sun, Gravity, and Position— This experiment relies on measurements from the inclinometers and sun sensor as well as knowledge of the rover position on the surface of the Earth. In our experiments, position is measured using the GPS, but even coarse localization is sufficient for a reasonable heading fix. Given this formulation,

(11) and (12) become

$$\mathbf{W} = \left[\begin{array}{cc} \mathbf{s}_S & \mathbf{g}_S \end{array} \right] \quad (21)$$

$$\mathbf{V} = \left[\begin{array}{cc} \mathbf{s}_F & \mathbf{g}_F \end{array} \right] \quad (22)$$

where we have used $(\forall i)\, a_i = 1$[1]. The best fit rotation, $\mathbf{C}_{SF}$, can be calculated from only a single pair of observations, but in practice, $\mathbf{g}_G$ is averaged over a short period (typically around 10 s), and converted to $\mathbf{g}_S$ using the calibration matrix, $\mathbf{C}_{SG}$. Multiple sun sensor readings can be averaged if taken over a short enough time, or simply appended to $\mathbf{W}$ (corresponding changes must be made to $\mathbf{V}$).

To extract the heading angle, α, from the $\mathbf{C}_{SF}$ matrix we first calculate $\mathbf{C}_{FT}$ from the known position using (4). Thus we can write

$$\mathbf{C}_{TS} = \mathbf{C}_{TF}\mathbf{C}_{FS} = \mathbf{C}_{FT}^T\mathbf{C}_{SF}^T \quad (23)$$

We know this equation will have the form given by (5). Multiplying out the component rotations gives a matrix of the form

$$\mathbf{C}_{TS} = \left[\begin{array}{ccc} c_\alpha c_\beta & c_\alpha s_\beta s_\gamma - s_\alpha c_\gamma & c_\alpha s_\beta c_\gamma + s_\alpha c_\gamma \\ s_\alpha c_\beta & -s_\alpha s_\beta s_\gamma + c_\alpha c_\gamma & -s_\alpha s_\beta c_\gamma - c_\alpha s_\gamma \\ -s_\beta & c_\beta s_\gamma & c_\beta c_\gamma \end{array} \right]. \quad (24)$$

Without loss of generality, we constrain β to the range $-\pi/2 \leq \beta \leq \pi/2$, and solve for α, the desired rover heading, from the components of $\mathbf{C}_{TS}$:

$$\beta = \text{asin}\left(-C_{TS_{31}}\right) \quad (25)$$

$$\alpha = \text{atan2}\left(C_{TS_{21}}/c_\beta, C_{TS_{11}}/c_\beta\right) \quad (26)$$

This experiment is convenient since it allows for rapid measurement of rover heading, with little impact on the time needed for an extended traverse.

Experiment 2: Heading from Sun and Position—Although heading can be obtained very rapidly using sun and gravity measurements, there are shortcomings to this approach. Inclinometers, especially inexpensive models, are prone to drift caused by temperature fluctutions and other factors. Figure 2 shows the history of the roll-axis, γ_G, over the course of a static nine-hour test. The low frequency change parallels the sun elevation from Figure 1, suggesting a possible temperature effect. To compensate for this effect we can reformulate the heading determination problem. Since the sun is not stationary, observations made over time will provide the necessary vectors to solve for orientation. In this case, (11) and (12) become

$$\mathbf{W} = \left[\begin{array}{cccc} \mathbf{s}_{S_1} & \mathbf{s}_{S_2} & \cdots & \mathbf{s}_{S_m} \end{array} \right], \quad (27)$$

$$\mathbf{V} = \left[\begin{array}{cccc} \mathbf{s}_{F_1} & \mathbf{s}_{F_2} & \cdots & \mathbf{s}_{F_m} \end{array} \right]. \quad (28)$$

Heading is obtained using (23)-(26), as in the previous case. Sun motion is relatively slow, so we must consider both the number of observations and the total measurement time required for a good heading fix.

[1] We will continue with unit weights for the rest of the paper.

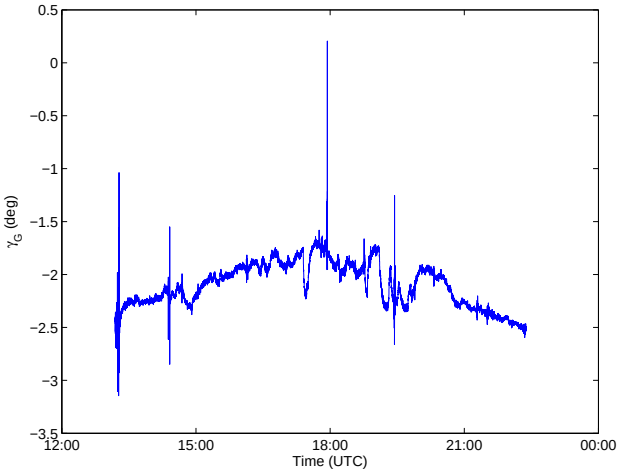

Figure 2. Roll angle drift during extended testing.

Experiment 3: Position and Heading from Sun and Gravity—Sun observations have historically been used for navigation; not just to measure heading, but also to determine latitude and longitude. In this experiment we reformulate the prior analysis to yield a simultaneous solution to global rover position as well as its heading.

To begin, we first solve for $\mathbf{C}_{SF}$ using any convenient formulation for $\mathbf{W}$ and $\mathbf{V}$. Our typical approach is to use a hybrid set of both sun and gravity vectors:

$$\mathbf{W} = \left[\begin{array}{ccccc} \mathbf{s}_{S_1} & \mathbf{s}_{S_2} & \cdots & \mathbf{s}_{S_m} & \mathbf{g}_S \end{array} \right] \quad (29)$$

$$\mathbf{V} = \left[\begin{array}{ccccc} \mathbf{s}_{F_1} & \mathbf{s}_{F_2} & \cdots & \mathbf{s}_{F_m} & \mathbf{g}_F \end{array} \right] \quad (30)$$

We now expand $\mathbf{C}_{SF} = \mathbf{C}_{ST}\mathbf{C}_{TF}$ in terms of principal axis rotations using (4) and (5):

$$\mathbf{C}_{SF}^T = \mathbf{R}_z\left(\lambda\right)\mathbf{R}_y\left(\frac{\pi}{2} - \phi\right)\mathbf{R}_z\left(\frac{\pi}{2} + \alpha\right)\mathbf{R}_y\left(\beta\right)\mathbf{R}_x\left(\gamma\right) \quad (31)$$

Postmultiply by $\mathbf{R}_x\left(-\gamma\right)\mathbf{R}_y\left(-\beta\right)$:

$$\mathbf{C}_{SF}^T\mathbf{R}_x\left(-\gamma\right)\mathbf{R}_y\left(-\beta\right) = \mathbf{R}_z\left(\lambda\right)\mathbf{R}_y\left(\frac{\pi}{2} - \phi\right)\mathbf{R}_z\left(\frac{\pi}{2} + \alpha\right) \quad (32)$$

If we calculate $\mathbf{g}_S$ from $\mathbf{g}_G$ using the calibration matrix, $\mathbf{C}_{SG}$, we can then extract the sun sensor's pitch, β, and roll, γ, angles using

$$\mathbf{g}_S = \left[\begin{array}{c} s_\beta \\ -c_\beta s_\gamma \\ -c_\beta c_\gamma \end{array} \right] \quad (33)$$

and compute the LHS of (32) above, assigning the result to a temporary rotation matrix, $\mathbf{C}$; the RHS of (32) is just a ZYZ Euler angle set, from which we can determine

$$\text{latitude:} \quad \phi = \frac{\pi}{2} - \text{acos}\left(C_{33}\right) \quad (34)$$

$$\text{longitude:} \quad \lambda = \text{atan2}\left(C_{23}/c_\phi, C_{13}/c_\phi\right) \quad (35)$$

$$\text{heading:} \quad \alpha = \text{atan2}\left(C_{32}/c_\phi, -C_{31}/c_\phi\right) - \frac{\pi}{2} \quad (36)$$

where C_{ij} are the elements of $\mathbf{C}$. The position estimate is quite coarse since small differences in ϕ and λ represent large

linear distances. In particular, errors in β and γ have a notable effect on positioning accuracy.

Self-Calibration

Although the sun sensor and inclinometer are both mounted to a common rigid plate, their body frames of reference may be different. Machining tolerances on the sensor head, or even clearance in a mounting hole can create a noticable difference between the two frames. In this section we provide a simple, and practical means of measuring $\mathbf{C}_{SG}$. This technique relies only on the sensors already integrated with the rover.

To proceed, we collect a series of n moderate-length sets of sun vector readings. Between datasets we reorient the rover in pitch and roll, ensuring that the sun remains in view. We do not need an external measure of β and γ. Using the estimation techniques of Experiment 2 we calculate $\mathbf{C}_{SF_j}$ for each dataset. Averaging the inclinometer readings gives us $\mathbf{g}_{G_j}$.

For each dataset, we use the known rover position to calculate $\mathbf{g}_F$ from (7), and transform these vectors into S:

$$\mathbf{g}_{S_j} = \mathbf{C}_{SF_j}\mathbf{g}_F \tag{37}$$

The solution for the calibration matrix $\mathbf{C}_{SG}$ follows from another application of the q-method using

$$\mathbf{W} = \begin{bmatrix} \mathbf{g}_{S_1} & \mathbf{g}_{S_2} & \cdots & \mathbf{g}_{S_n} \end{bmatrix}, \tag{38}$$

$$\mathbf{V} = \begin{bmatrix} \mathbf{g}_{G_1} & \mathbf{g}_{G_2} & \cdots & \mathbf{g}_{G_n} \end{bmatrix}. \tag{39}$$

The lack of reliance on external measurements makes this approach attractive, but this method is still limited by inclinometer drift. This method has performed adequately in our initial studies, but we are investigating strategies for improving the accuracy of this calibration.

4. Field Testing

To prove out our sun sensing algorithms, we conducted a set of field trials at two distinct sites with a sun sensor originally designed for attitude determination on microsatellites. Below we describe the experimental setup, our datasets, and our means of determining ground truth heading in the field.

Test Locations

The datasets used in the experiments described in this paper were collected at two locations: the Haughton-Mars Project Research Station (HMPRS) ($75°22'$ N latitude and $89°41'$ W longitude) and the University of Toronto Institute for Aerospace Studies (UTIAS) ($43°47$ N latitude and $79°28'$ W longitude). The HMPRS is situated just outside the northwest area of the Haughton impact crater, on Devon Island, in the Canadian High Arctic [18]. Haughton presents unique qualities for planetary analog studies because it offers an unusually wide variety of geological features and microbiological attributes of strong planetary analog value or potential. Haughton is also in a polar desert environment, which presents real challenges to field exploration that are analogous in fundamental ways to those expected in planetary exploration. It is worth pointing out that our Devon tests were conducted in July 2008, at which time the sun remained above the horizon 24 hours a day. Also, due to the high latitude of this site, it provides a good proving ground for sun sensor localization methods intended for use at, for example, the lunar poles. This site has been used for rover testing in the past [19], [20], [21], [22].

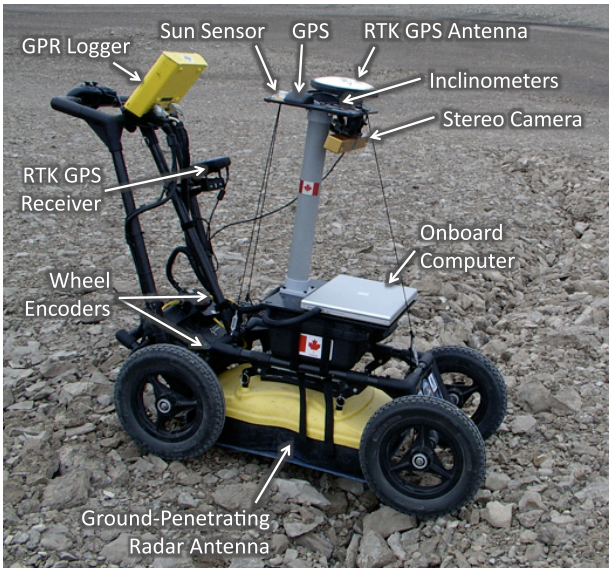

Figure 3. The rover platform (shown here on Devon Island).

Rover Platform

The data for the experiments in this paper were collected by a pushcart rover platform developed at the University of Toronto Institute for Aerospace Studies and shown in Figure 3. The platform includes rover engineering sensors (i.e., stereo camera, inclinometers, sun sensor, wheel odometers), a ground-penetrating radar, an on-board computer, and two independent GPS systems (one Real-Time Kinematic) used for ground-truth positioning. Although this was not an actuated rover, our focus with this platform is on problems of estimation (e.g., [23]), and thus it was entirely sufficient as a means to gather data. The sun sensor was a Sinclair Interplanetary SS-411 and is described in more detail below. The inclinometer was a Honeywell HMR-3000. The stereo camera was a Point Gray Research Bumblebee XB3 with a 24 cm baseline and $70°$ field of view, mounted approximately 1 m above the surface pointing downward by approximately $20°$.

The SS-411 Sun Sensor

The sun sensor used in this study is a Sinclair Interplanetary SS-411 digital sun sensor. It is a very small (30 g), low-power device. It boasts a $0.1°$ (1-σ) accuracy over a $70°$ half-angle field of view. An integrated microcontroller processes the readings from a linear pixel array and outputs the floating-point sun-vector in sensor coordinates. In previous studies

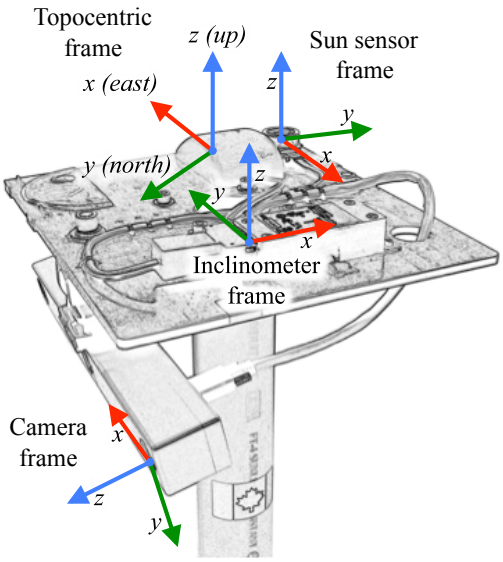

Figure 4. Frames associated with the sensor head. Clockwise from top-left: the topocentric frame, T, (x east, y north); the sun sensor frame, S; the inclinometer frame, G; and the camera frame, C.

[24], we detail the development of the sun estimation routines used in the embedded processor.

The algorithms on this device assess the quality of the detector image for each sensor measurement. Poor quality output will cause the sensor to flag the sun vector estimates as unreliable, or invalid. This behaviour appears in the collected datasets as intermittent or extended gaps in the sensor data. Clouds were the most common cause of this problem. More problematic were readings that showed strong cloud reflections close to the sun itself. These situations introduce substantial biases into the measurements.

Short Datasets

For the evaluation of Experiment 1, short datasets were collected at 23 locations on Devon Island. At each location, readings from the sun sensor, inclinometer, and GPS were logged for approximately 10 seconds. As this site is near the magnetic north pole, we were unable to use a magnetic compass to obtain ground-truth heading. Instead, we devised a method of measuring the heading of the sensor using GPS. We deployed a target approximately 100 m from the sensor head, surveyed the position of the target and imaged it with the stereo camera. Converting the GPS locations to Universal Transverse Mercator (UTM) coordinates, we define $\mathbf{x}_s = [x_s \; y_s]^T$ to be the measured position of the rover and $\mathbf{x}_t = [x_t \; y_t]^T$ to be the measured position of the target. The x and y coordinates correspond to easting and northing, respectively. The surveyed points are used to calculate θ, a known bearing in the topocentric frame:

$$\theta = \text{atan2}(y_t - y_s, x_t - x_s) \tag{40}$$

Choosing the location of the target in one of the stereo images determines the bearing of the target with respect to the camera. Finally, the known transformation between the stereo camera and the sun sensor, $\mathbf{C}_{SC}$, which we currently obtain from the geometry of the sensor head, determines the heading of the sun sensor, α_{true}.

As we are using θ as ground-truth, it is useful to examine the accuracy this method can hope to achieve. For a generic position measurement, $\mathbf{x}_i$, we model the measurement noise, $\delta\mathbf{x}_i$, as drawn from a zero-mean Gaussian density with covariance $\mathbf{\Sigma}_i$:

$$\delta\mathbf{x}_i \sim \mathcal{N}(\mathbf{0}, \mathbf{\Sigma}_i) \tag{41}$$

The components of $\delta\mathbf{x}_i$ are defined to be

$$\delta\mathbf{x}_i = \begin{bmatrix} \delta x_i \\ \delta y_i \end{bmatrix} \tag{42}$$

and the components of $\mathbf{\Sigma}_i$ are

$$\mathbf{\Sigma}_i = \begin{bmatrix} \sigma^2_{xx,i} & \sigma^2_{xy,i} \\ \sigma^2_{xy,i} & \sigma^2_{yy,i} \end{bmatrix} \; . \tag{43}$$

The value of $\mathbf{\Sigma}_i$ is determined by the properties of our GPS unit. The noise model allows us to define

$$\mathbf{x}_i = \bar{\mathbf{x}}_i + \delta\mathbf{x}_i \tag{44}$$

where $\bar{\mathbf{x}}_i = [\bar{x}_i \; \bar{y}_i]^T$ is the true position of the object.

To evaluate the accuracy of θ, we rewrite (40)

$$(x_t - x_s)\sin\theta = (y_t - y_s)\cos\theta$$

which we expand to

$$\begin{aligned}&(\bar{x}_t + \delta x_t - \bar{x}_s - \delta x_s)\sin(\bar{\theta} + \delta\theta) \\ &\quad = (\bar{y}_t + \delta y_t - \bar{y}_s - \delta y_s)\cos(\bar{\theta} + \delta\theta) \; .\end{aligned} \tag{45}$$

Assuming $\delta\theta$ is small, we may approximate the perturbation by a first-order Taylor expansion:

$$\begin{aligned}&(\bar{x}_t + \delta x_t - \bar{x}_s - \delta x_s)\left(\sin\bar{\theta} + \cos\bar{\theta}\delta\theta\right) \\ &\quad \approx (\bar{y}_t + \delta y_t - \bar{y}_s - \delta y_s)\left(\cos\bar{\theta} - \sin\bar{\theta}\delta\theta\right)\end{aligned} \tag{46}$$

In the absence of noise, the true heading, $\bar{\theta}$ satisfies

$$(\bar{x}_t - \bar{x}_s)\sin\bar{\theta} = (\bar{y}_t - \bar{y}_s)\cos\bar{\theta} \; . \tag{47}$$

Subtracting the operating point, (47), from (46), and assuming that products of small terms are zero, approximates the resulting perturbation:

$$\begin{aligned}&(\delta x_t - \delta x_s)\sin\bar{\theta} + (\bar{x}_t - \bar{x}_s)\cos\bar{\theta}\delta\theta \\ &\quad = (\delta y_t - \delta y_s)\cos\bar{\theta} - (\bar{y}_t - \bar{y}_s)\sin\bar{\theta}\delta\theta\end{aligned} \tag{48}$$

which we solve for $\delta\theta$:

$$\delta\theta = \frac{(\delta y_t - \delta y_s)\cos\bar{\theta} - (\delta x_t - \delta x_s)\sin\bar{\theta}}{(\bar{x}_t - \bar{x}_s)\cos\bar{\theta} + (\bar{y}_t - \bar{y}_s)\sin\bar{\theta}} \tag{49}$$

The denominator of $\delta\theta$ is $\bar{d}$, the distance between the two points, such that we may write

$$\delta\theta = \frac{(\delta y_t - \delta y_s)\cos\bar{\theta} - (\delta x_t - \delta x_s)\sin\bar{\theta}}{\bar{d}} \quad . \tag{50}$$

From this expression, we can examine the resulting properties of $\delta\theta$. Its mean is

$$\begin{aligned} E(\delta\theta) &= E\left(\frac{(\delta y_t - \delta y_s)\cos\bar{\theta} - (\delta x_t - \delta x_s)\sin\bar{\theta}}{\bar{d}}\right) \\ &= \frac{E(\delta y_t - \delta y_s)\cos\bar{\theta} - E(\delta x_t - \delta x_s)\sin\bar{\theta}}{\bar{d}} \\ &= 0 \end{aligned} \tag{51}$$

where $E(\cdot)$ is the expectation operator. Assuming that individual measurements are independent (i.e., $E(\delta\mathbf{x}_s\delta\mathbf{x}_t^T) = \mathbf{0}$), we solve for the variance $\sigma_\theta^2 = E(\delta\theta^2)$:

$$\sigma_\theta^2 = \frac{v_{xx} + v_{yy} + v_{xy}}{\bar{d}^2} \tag{52}$$

where we define the terms in the numerator:

$$\begin{aligned} v_{xx} &= (\sigma_{yy,t}^2 + \sigma_{yy,s}^2)\cos^2\bar{\theta} \\ v_{yy} &= (\sigma_{yy,t}^2 + \sigma_{yy,s}^2)\sin^2\bar{\theta} \\ v_{xy} &= (\sigma_{xy,t}^2 + \sigma_{xy,s}^2)\sin 2\bar{\theta} \end{aligned} \tag{53}$$

We assume that our GPS units are subject to isotropic noise:

$$\mathbf{\Sigma}_t = \sigma_t^2\mathbf{1} \tag{54}$$

$$\mathbf{\Sigma}_s = \sigma_s^2\mathbf{1} \tag{55}$$

where $\mathbf{1}$ is the identity matrix. Under this assumption, σ_θ^2 simplifies to

$$\sigma_\theta^2 = \frac{\sigma_t^2 + \sigma_s^2}{\bar{d}^2} \quad . \tag{56}$$

Thus, knowing the properties of our GPS units (σ_t and σ_s) allows us to estimate the accuracy of our ground-truth heading using (56). We used a handheld GPS unit to survey the target, $\mathbf{x}_t$, and a real-time kinematic GPS to survey the rover's position, $\mathbf{x}_s$. Devon Island is at a high latitude and the GPS satellites are low on the horizon so we estimate $\sigma_t = 2$ and $\sigma_s = 0.4$.

Long Datasets

Three long datasets were collected, two on Devon Island (`devonStatic1`, `devonStatic2`) and one at the University of Toronto (`utias9h`). For each dataset, the rover logged sun data, inclinometer, and GPS for a number of hours. For the `utias9h` dataset, ground-truth heading was surveyed using the method described in Section 4. Table 2 summarizes these long datasets.

5. RESULTS

This section presents our results for Experiments 1, 2, and 3. In what follows, heading error, $\delta\alpha$, is computed as

$$\delta\alpha = \alpha - \alpha_{\text{true}} \tag{57}$$

where α is our estimate of rover heading and α_{true} is the ground-truth.

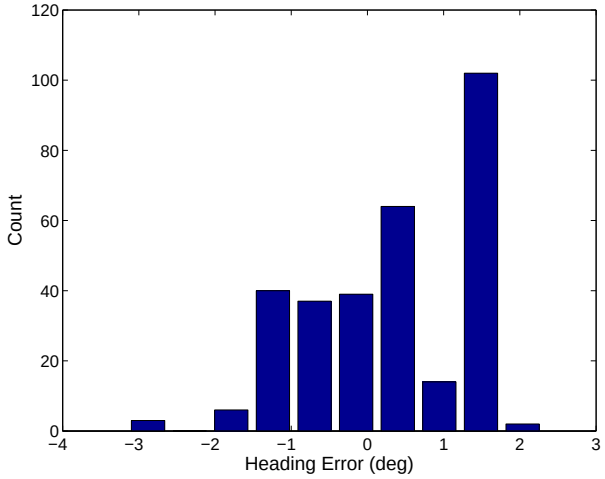

Figure 5. Experiment 1: Heading from sun, gravity and position. A summary of the heading error on the 307 measurements from different sites on Devon Island.

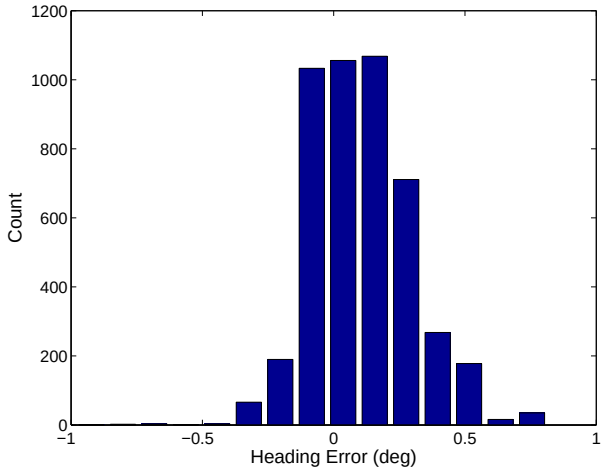

Figure 6. Experiment 1: Heading from sun, gravity and position. A summary of the heading error on the 4635 measurements in the `utias9h` dataset.

Experiment 1: Heading from Sun, Gravity, and Position

We initially used the 'Short Datasets' for this experiment. The distance between the rover and target ranged from $\bar{d} = 80$ m to $\bar{d} = 148$ m resulting in a ground-truth heading accuracy of between $\sigma_\theta = 1.47°$ and $\sigma_\theta = 0.79°$. Between 4 and 31 sun vectors were processed at each of 23 sites resulting in 307 data points. The mean heading error is $\overline{\delta\alpha} = 0.287°$ and the standard deviation is $\sigma_\alpha = 1.02°$. A histogram of the errors is shown in Figure 5. Because the heading errors were on par with the uncertainty in our ground truth measurement, a more accurate measure of ground-truth would be necessary to evaluate the method further.

We also applied our method to the `utias9h` dataset, which is 9 hours long and has ground-truth heading ($\sigma_\theta = 0.8°$). We ran this experiment on each of the 4635 measurements from this dataset. The algorithm exhibits a mean error of $\overline{\delta\alpha} =$

Table 2. A summary of static datasets.

Dataset	*Position*	*Ground-Truth* α_{true}	*Start (UTC)*	*Stop (UTC)*	*# Sun Vectors*
`utias9h`	43.782 N, 79.466 W	Y	2008-09-10 13:11:42	2008-09-10 21:48:53	4635
`devonStatic1`	75.433 N, 89.864 W	N	2008-07-11 15:00:22	2008-07-12 01:33:12	33561
`devonStatic2`	75.433 N, 89.864 W	N	2008-07-13 13:36:18	2008-07-13 20:42:52	2138

Table 3. Experiment 2 results from `utias9h` dataset.

Δt_w (min.)	Batches	$\overline{\delta\alpha}$ (deg.)	σ_α (deg)
5	65	0.27	4.02
10	32	0.08	2.28
15	21	0.17	1.11
20	16	0.08	0.66
25	13	0.20	0.72
30	10	0.13	0.42
60	5	0.02	0.27

$0.106°$ and a standard deviation of $\sigma_\alpha = 0.196°$. A histogram of the results is shown in Figure 6.

Experiment 2: Heading from Sun and Position

Our objectives in conducting this experiment are twofold: we wish to compare the achievable accuracy of the heading determination to the results of Experiment 1 and we also wish to evaluate the how long we must observe to attain an acceptable heading fix. We consider the three static tests (see Table 2). Even though we do not have heading ground-truth data for the `devonStatic1` and `devonStatic2` tests, the standard deviation in the resulting estimates give useful information.

To process the data, we divided the observations into non-overlapping time windows of length Δt_w. All observations from within a time window were used to estimate α. Mean error, $\overline{\delta\alpha}$, and standard deviation, σ_α, for the `utias9h` dataset are shown in Table 3. Windows with an insufficient number of data points have been omitted from these calculations. The most common cause of missing data was cloud cover (see Figure 1). The mean error and standard deviation both drop as the integration time increases (it should be noted that the small number of long datasets makes our *estimates* of $\overline{\delta\alpha}$ and σ_α uncertain). The trend in the mean error is somewhat perplexing, but from the distribution of errors (Figure 7), we see the bias in heading seems to be driven by outliers, rather than a systematic error in all the estimates. The outliers correlate with sun estimates that have been corrupted by cloud-cover.

We can apply similar analysis to the two Devon Island datasets. If we assume that the estimates remain zero-mean, then performance will be governed by the standard deviation, σ_α. Results from the three long tests are shown in Figure 8. All of the curves follow a similar trend. We attribute the high initial σ_α values in the `utias9h` dataset to the sporadic cloud cover observed during the test; the slightly elevated initial values during the `devonStatic2` test could be blamed on the observed haze, but the results are inconclusive. Further tests are necessary to provide additional validation, but the results are quite encouraging from an operational standpoint. On a clear day, a five minute observation will give a 1-σ fix of about $2°$ and at twenty minutes, the error drops to about $1°$. The Experiment 1 technique appears to be a much faster method of measuring heading, but the two techniques perform similarly when Δt_w increases to about an hour.

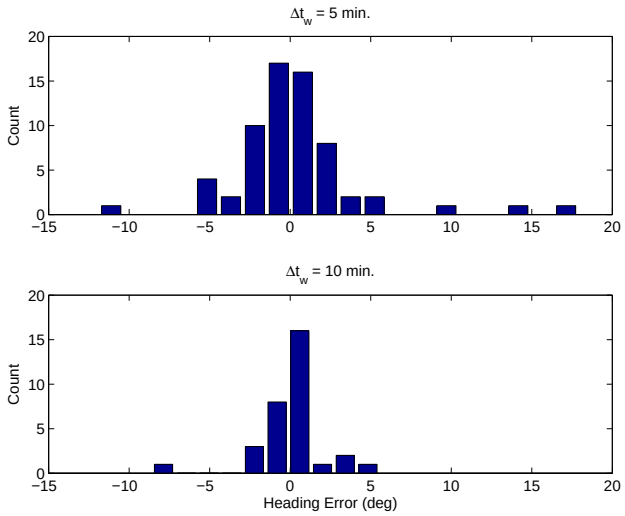

Figure 7. Experiment 2: Error distribution for `utias9h` dataset. Results are shown for 5 and 10 minute windows.

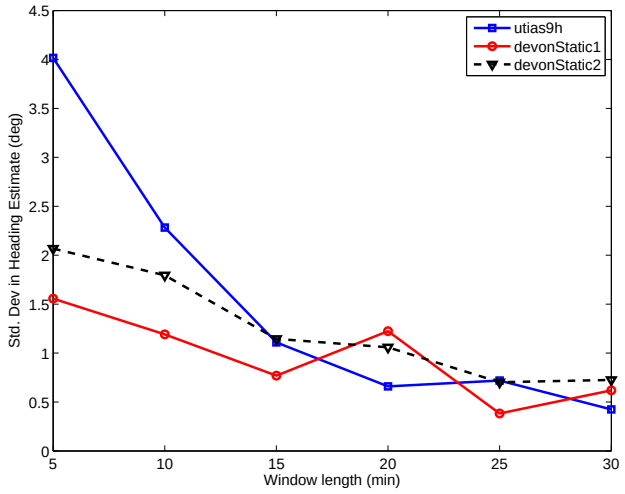

Figure 8. Experiment 2: Effect of window length on heading estimates.

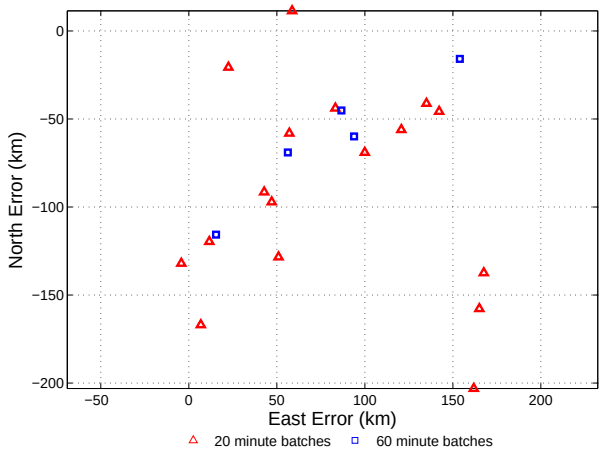

Figure 9. Experiment 3: Global position error running batches on the `utias9h` dataset.

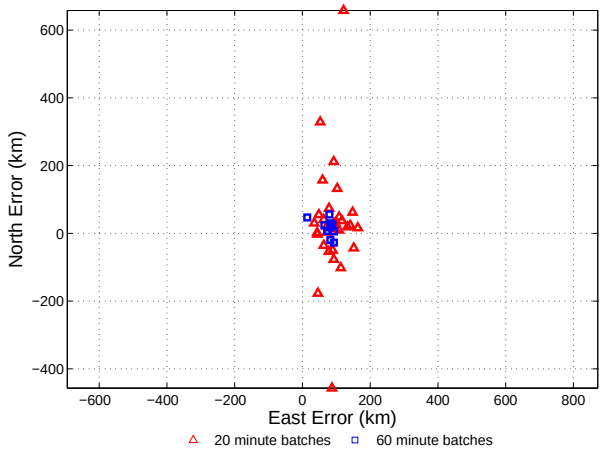

Figure 10. Experiment 3: Global position error running batches on the `devonStatic1` dataset.

Experiment 3: Position and Heading from Sun and Gravity

The results for Experiment 3 are very preliminary. Batches of sun vectors were processed to obtain $\mathbf{C}_{SF}$ and the gravity vector was used to estimate the latitude and longitude of the rover. The resulting coordinates were converted to UTM to plot the estimation errors. The results are plotted in Figures 9 to 11. In general, the errors are below 200 km and increasing the batch size reduces the error. Although these preliminary results are not good enough to use for rover navigation alone, this still represents a reasonable estimate of global location on a planet using very inexpensive sensors and with no a priori knowledge of position. The output of this algorithm could be used as an initial guess for a local refinement by another method.

6. Conclusions & Future Work

This paper has presented an experimental study of sun sensing as a rover navigational aid. Our sensor suite consists of a sun sensor, inclinometer, and clock (as well as ephemeris data). We described two techniques to determine

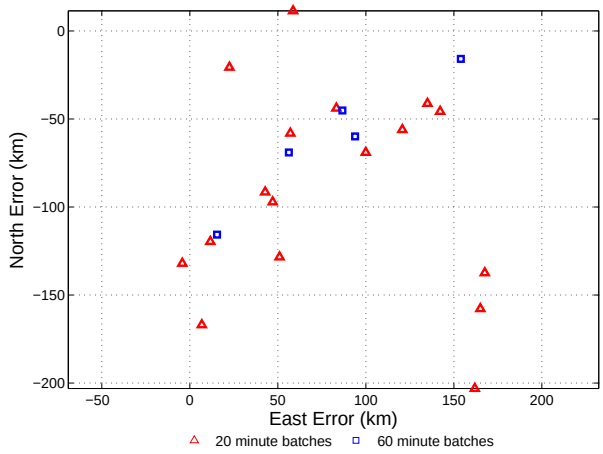

Figure 11. Experiment 3: Global position error running batches on the `devonStatic2` dataset.

rover heading (one involving the inclinometer and the other without). Both techniques are capable of producing heading estimates accurate to within a few degrees. The main difference is that the technique that does not use an inclinometer requires a fairly long window of sun sensor data (e.g., 1 hour) to obtain this accuracy. The novel contributions of our paper (for rover heading determination) are:

(i) Extensive experimental results (i.e., our datasets were collected at two very different sites on Earth and contain thousands of sun vectors).
(ii) A method to self-calibrate the relative orientation between the sun sensor and inclinometer sensors.
(iii) A method to obtain ground-truth rover heading in the field (i.e., we do not employ a magnetic compass) and a means to predict its accuracy.
(iv) Studies of the effect of sun sensor window length on the resulting heading estimate accuracy.

Our results are also unique in that we employed the Sinclair Interplanetary SS-411 sun sensor, a real space-grade satellite sensor that requires little in the way of power and data processing. However, our methodology could also be applied to a camera-based sun sensor. Heading and position estimates are very sensitive to errors in the sun vector measurement caused by atmospheric effects such as clouds and haze. Optimizing the sensor processing for terrestrial applications may improve performance in marginal operating conditions.

The paper also reported preliminary results on determining global position of a rover using our sensor suite. The results are encouraging, but not yet adequate to be used alone for global positioning (i.e., errors are as large as 200 km). Even accounting for the difference in radii of the Earth and moon, this error would be too large for practical use. Future work on global position determination will include more sophisticated error modeling and evaluation of our formulation against the "circles of equal altitude" algorithm [12]. We will also investigate the possibility of obtaining a more accurate inclinome-

ter, accounting for temperature effects, and more accurately calibrating the transformations between frames in the sensor suite itself.

Finally, we hope to extend our work to allow the use of long windows of sun vectors collected from a moving rover platform. Our long-duration tests showed significant benefit may be gained by employing a large window of sun sensor observations. However, it may not be practical to wait several hours simply to determine rover heading. One promising concept is to integrate the sun sensor with our work on visual odometry [23] to estimate both relative and absolute position/orientation simultaneously.

ACKNOWLEDGMENTS

The authors would like to thank Mr. Doug Sinclair of Sinclair Interplanetary for the donation of a SS-411 Digital Sun Sensor. Funding for this work was provided in part by the Natural Sciences and Engineering Research Council (NSERC) of Canada. Funding for our field trials on Devon Island was provided by the Canadian Space Agency's Canadian Analogue Research Network (CARN) program. Thanks to the Mars Institute and the Haughton-Mars Project for providing infrastructure on Devon Island. The authors are grateful to the members of the communities of Resolute Bay, Grise Fjord, and Pond Inlet who acted as guides on Devon Island. Finally, at the University of Toronto Institute for Aerospace Studies, Patrick Carle helped with the creation of our ground-truth heading system, Konstantine Tsotsos and Peter Miras provided logistical support, and Rehman Merali pitched in during assembly of our pushcart rover.

REFERENCES

[1] B. Wilcox and T. Nguyen, "Sojourner on mars and lessons learned for future planetary missions," in *Proceedings of the 28th International Conference on Environmental Systems (ICES), Society of Automotive Engineers (SAE)*, Danvers, Massachusetts, 13-16 July 1998.

[2] A. Eisenman, C. Liebe, and R. Perez, "Sun sensing on the mars exploration rovers," *Aerospace Conference Proceedings, 2002. IEEE*, vol. 5, pp. 5–2249–5–2262 vol.5, 2002.

[3] K. S. Ali, C. A. Vanelli, J. J. Biesiadecki, M. W. Maimone, A. Yang Cheng, M. San Martin, and J. W. Alexander, "Attitude and position estimation on the mars exploration rovers," *IEEE Systems, Man and Cybernetics, International Conference*, vol. 1, pp. 20– 27, October 2005.

[4] M. Shuster and S. Oh, "Three-axis attitude determination from vector observations," *Journal of Guidance and Control*, vol. 4, no. 1, pp. 70–77, 1981.

[5] M. W. Maimone, P. C. Leger, and J. J. Biesiadecki, "Overview of the mars exploration rovers' autonomous mobility and vision capabilities," in *IEEE International Conference on Robotics and Automation (ICRA) Space Robotics Workshop*, April 2007.

[6] Y. Kuroda, T. Kurosawa, A. Tsuchiya, and T. Kubota, "Accurate localization in combination with planet observation and dead reckoning for lunar rover," *Robotics and Automation, 2004. Proceedings. ICRA '04. 2004 IEEE International Conference on*, vol. 2, pp. 2092–2097 Vol.2, 26-May 1, 2004.

[7] R. Volpe, "Mars rover navigation results using sun sensor heading determination," in *Intelligent Robots and Systems, 1999. IROS '99. Proceedings. 1999 IEEE/RSJ International Conference on*, vol. 1, 1999, pp. 460–467.

[8] A. Trebi-Ollennu, T. Huntsberger, Y. Cheng, E. Baumgartner, B. Kennedy, and P. Schenker, "Design and analysis of a sun sensor for planetary rover absolute heading detection," *Robotics and Automation, IEEE Transactions on*, vol. 17, no. 6, pp. 939–947, 2001.

[9] D. Sigel and D. Wettergreen, "Star tracker celestial localization system for a lunar rover," *Intelligent Robots and Systems, 2007. IROS 2007. IEEE/RSJ International Conference on*, pp. 2851–2856, 29 2007-Nov. 2 2007.

[10] M. Deans, D. Wettergreen, and D. Villa, "A Sun Tracker for Planetary Analog Rovers," in *'i-SAIRAS 2005' - The 8th International Symposium on Artificial Intelligence, Robotics and Automation in Space*, ser. ESA Special Publication, vol. 603, Aug. 2005.

[11] C. Pingyuan, Y. Fuzhan, and C. Hutao, "Attitude and position determination scheme of lunar rovers basing on the celestial vectors observation," in *Integration Technology, 2007. ICIT '07. IEEE International Conference on*, 2007, pp. 538–543.

[12] F. Cozman and E. Krotkov, "Robot localization using a computer vision sextant," in *IEEE International Conference on Robotics and Automation*, vol. 1, May 1995, pp. 106–111.

[13] D. A. Vallado and W. D. McClain, *Fundamentals of Astrodynamics and Applications*, 3rd ed. Microcosm Press, 2007.

[14] J. H. Meeus, *Astronomical Algorithms*. Willmann-Bell, Incorporated, 1991.

[15] G. Wahba, "A least squares estimate of satellite attitude," *SIAM Review*, vol. 7, p. 409, 1965.

[16] P. Davenport, "A vector approach to the algebra of rotations with applications," NASA Technical Note TN D-4696, Aug. 1968.

[17] F. L. Markley and D. Mortari, "How to estimate attitude from vector observations," *AAS Paper*, pp. 99–427.

[18] P. Lee, S. Braham, M. Boucher, J. Schutt, B. Glass, A. Gross, B. Hine, C. McKay, S. Hoffman, J. Jones, A. Berinstain, J.-M. Comptois, E. Hodgson, and N. Wilkinson, "Haughton-mars project: 10 years of science operations and exploration systems development at a moon/mars analog site on devon island, high arctic,"

in *Proceedings of the 38th Lunar and Planetary Science Conference*, League City, Texas, March 12-16 2007, pp. 2426–2427.

[19] D. Wettergreen, M. Dias, B. Shamah, J. Teza, P. Tompkins, C. Urmson, M. Wagner, and W. Whittaker, "First experiment in sun-synchronous exploration," in *Proceedings of the IEEE International Conference on Robotics and Automation (ICRA)*, Washington, DC, May 2002, pp. 3501–3507.

[20] D. Wettergreen, P. Tompkins, C. Urmson, M. Wagner, and W. Whittaker, "Sun-synchronous robotic exploration: Technical description and field experimentation," *International Journal of Robotics Research*, vol. 24, no. 1, pp. 3–30, 2005.

[21] T. Fong, M. Deans, P. Lee, and M. Bualat, "Simulated lunar robotic survey at terrestrial analog sites," in *Proceedings of the 38th Lunar and Planetary Science Conference*, League City, Texas, March 12-16 2007.

[22] T. Fong, M. Allan, X. Bouyssounouse, M. Bualat, M. Deans, L. Edwards, L. Fluckiger, L. Keely, S. Lee, D. Lees, V. To, and H. Utz, "Robotics site survey at haughton crater," in *Proceedings of the 9th International Symposium on Artificial Intelligence, Robotics and Automation in Space (iSAIRAS)*, Los Angeles, CA, February 26-29 2008.

[23] P. Furgale, T. Barfoot, N. Ghafoor, T. Haltigin, K. Williams, and G. Osinski, "Field testing of an integrated surface/subsurface modeling technique for planetary exploration," October 2008, manuscript submitted to the International Journal of Robotics Research special issue on Computer Vision.

[24] J. Enright and D. Sinclair, "Algorithm enhancements for the ss-411 digital sun sensor," in *Proc. of the 21st AIAA/USU Conference on Small Satellites*, Aug. 2007.

BIOGRAPHY

John Enright holds a BASc (1997) from the University of Toronto (Engineering Science: Aerospace) and a MS (1999) and a PhD (2002) from MIT in Aerospace Systems. He is currently an Associate Professor in Aerospace Engineering at Ryerson University in Toronto. Having joined the faculty at Ryerson University in 2003, he is now the Principal Investigator of the Space Avionics and Instrumentation Laboratory (SAIL). While at MIT (1999-2003), he led the software development for the SPHERES flight project, and the GFLOPS real-time spacecraft simulation testbed. His research interests include spacecraft avionics and sensor processing, systems engineering and flight software. Dr. Enright is a member of the AIAA, CASI, and the IEEE.

Paul Furgale received his BASc (2006) from the University of Manitoba (Computer Science) and is now a PhD Student in the Autonomous Space Robotics Lab at the University of Toronto Institute for Aerospace Studies (UTIAS). His research interests include computer vision and localization technology for planetary exploration rovers.

Tim Barfoot holds a BASc (1997) from the University of Toronto (Engineering Science: Aerospace) and a PhD (2002) from the University of Toronto Institute for Aerospace Studies (UTIAS) in Aerospace Engineering. He is currently an Assistant Professor at UTIAS, where he leads the Autonomous Space Robotics Lab. Before joining UTIAS, he worked at MDA Space Missions in the Controls & Analysis Group on applications of mobile robotics to space exploration and underground mining. Dr. Barfoot is a Canada Research Chair (Tier II) in Autonomous Space Robotics and a Professional Engineer (Ontario).